

pubs.acs.org/JPCC Article

Influence of APTES-Decorated Mesoporous Silica on the Dynamics of Ethylene Glycol Molecules—Insights from Variable Temperature ²H Solid-State NMR

Nadia B. Haro Mares, Martin Brodrecht, Till Wissel, Sonja C. Döller, Lorenz Rösler, Hergen Breitzke, Markus M. Hoffmann, Torsten Gutmann,* and Gerd Buntkowsky*



Cite This: https://doi.org/10.1021/acs.jpcc.3c03671



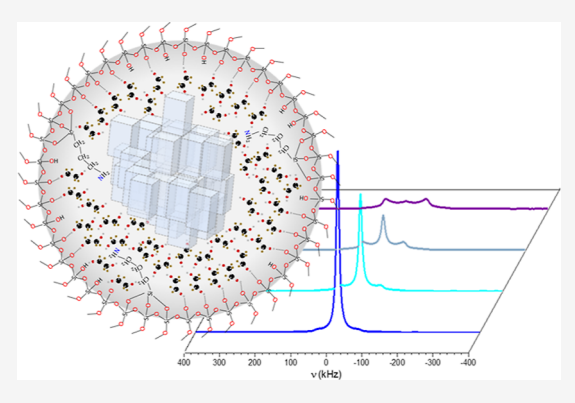
ACCESS I

III Metrics & More

Article Recommendations

Supporting Information

ABSTRACT: The physicochemical effects of decorating pore walls of high surface area materials with functional groups are not sufficiently understood, despite the use of these materials in a multitude of applications such as catalysis, separations, or drug delivery. In this study, the influence of 3-amino-propyl triethoxysilane (APTES)-modified SBA-15 on the dynamics of deuterated ethylene glycol (EG- d_4) is inspected by comparing three systems: EG- d_4 in the bulk phase (sample 1), EG- d_4 confined in SBA-15 (sample 2), and EG- d_4 confined in SBA-15 modified with APTES (sample 3). The phase behavior (i.e., melting, crystallization, glass formation, etc.) of EG- d_4 in these three systems is studied by differential scanning calorimetry. Through line shape analysis of the 2 H solid-state NMR (2 H ssNMR) spectra of the three systems recorded at different temperatures, two signal patterns, (i) a Lorentzian (liquid-like) and (ii) a Pake pattern (solid-like), are identified



from which the distribution of activation energies for the dynamic processes is calculated employing a two-phase model.

■ INTRODUCTION

Mesoporous silica materials have been the subject of many studies in the past decades. Their characteristic properties, such as high thermal stability, large surface area, nontoxicity, and good availability, make them suitable for various applications. For example, these materials are applied in ion exchangers, molecular sieves, adsorption media, optics, catalysis, bioengineering, energy storage, or drug delivery systems. One of the many features of mesoporous silica materials is the tunable size of their pores, typically between 2 and 50 nm, which gives them a high specific inner surface area. A,8,9

For the specific application of porous silica materials in heterogeneous catalysis, drug delivery, and ion conductors, it is necessary to modify the pore surfaces by covalent attachment of organic molecules to the silanol groups at the silica pore walls in many cases. ^{10–12} Such functionalization changes the hydrophilicity of the surface and, thus, the chemical affinities toward molecules inside the pores. ^{13–18} The dynamics of guest molecules in the direct vicinity of the pore walls are affected by the geometry and chemical nature of the walls. These perturbations are noticed by a change in mobility of the guest molecules, ^{2,19} which in turn influences thermodynamic processes such as melting, freezing, adsorption, or desorption. ²⁰ These so-called confinement effects have been extensively studied for water and small organic molecules in porous silica. ^{21–25}

Three-aminopropyl triethoxysilane (APTES) is one of the most widely used functionalization agents to modify silica surfaces since the presence of the terminal amine group ($-\mathrm{NH}_2$) allows attaching or "linking" moieties of interest such as drugs, biomolecules (enzymes, DNA, proteins, etc.), and homogeneous transition metal catalysts. ^{26–28} Specifically, amine groups are suitable to form covalent amide bonds by reaction with carboxyl moieties that enable them to bind amino acids or peptides. ²⁹ Two complementary approaches are known to incorporate APTES linker groups into silica materials: (i) the linker molecule can be attached to the silanol groups in the pores of the material via covalent binding after the mesoporous material is synthesized (grafting approach), or (ii) the linker molecule can be tethered during the synthesis of the material (co-condensation approach). ³⁰

The interest in studying the dynamics of molecules in confinement has increased significantly in the past few years. Among these, ethylene glycol (EG) and its derivatives are relevant systems to be studied.^{31–33} This type of solvent, which

Received: May 31, 2023
Revised: September 12, 2023



is widely used in industrial processes, has the big advantage of being considered "green", due to its low toxicity, nonvolatility, high abundance, and availability from biomass. 34–37 Such broad application potential necessitates deeper knowledge of the structural arrangement of EG in chemical environments, such as inside the pores of modified porous silica. The analysis of the structural arrangement of EG under confinement is a challenging task given that neat EG is present in coexistent glassy and crystalline phases. 38

To explore the impact of confinement effects and to inspect the influence of the APTES modification of the pore surface on the structure and dynamics of ethylene glycol, a combination of differential scanning calorimetry (DSC) and variable-temperature ²H solid-state NMR (²H ssNMR) is suitable, as recently demonstrated for 1-octanol in porous silica by some of the authors.³⁹ DSC provides information on physical processes such as melting, crystallization, or glass transitions of ethylene glycol in a confined environment. $^{40-43}$ Solid-state NMR provides information on the onset of rovibrational motions, which may occur at temperatures different from the macroscopic phase transitions. 19,44 Insights into dynamics are accessible by extracting NMR parameters encoded in the line shape of the spectra recorded at different temperatures. For example, the use of quadrupolar nuclei such as deuterium allows for the analysis of intramolecular motions in deuterated molecules via changes in the ²H ssNMR line shapes. ^{45–47} Thus, the combination of DSC and ²H ssNMR allows for studying the behavior of the ethylene glycol inside the pores of silica materials and inspecting the impact of the APTES functionalization on the structure and dynamics of the ethylene glycol in confinement.

For this study, two Santa Barbara Amorphous materials (SBA) are used as confinement models: SBA-15 modified with APTES groups attached to the pore walls via co-condensation and pure SBA-15 as a reference. Partially deuterated ethylene glycol (EG- d_4), where the OH-groups are nondeuterated, serves as a guest molecule in our study. This is important since OHgroups easily exchange their hydrogen in the presence of other available hydrogens, i.e., from the surface silanol groups or the amine group of the APTES linker in the case of the confined samples. Such exchange processes would complicate the line shape analysis of the spectra and the description of the dynamics of the molecules. First, the three systems $[EG-d_4]$ in the bulk phase (sample 1), EG- d_4 confined in pure SBA-15 (sample 2), and EG- d_4 confined in SBA-15 modified with APTES (sample 3)] are analyzed via DSC to obtain information on physical processes (i.e., melting, crystallization, glass formation, etc.) in these systems. An extensive study is then performed by variabletemperature ²H ssNMR. The results are presented and discussed to derive a detailed picture of how APTES functional groups affect the dynamics of EG- d_4 in porous silica materials.

■ EXPERIMENTAL SECTION

General. If not explicitly mentioned, all chemicals were used without further purification. Pluronic P123 ($M_{\rm n} \sim 5800$) was purchased from Sigma-Aldrich. Hydrochloric acid (37 wt %, HCl) and ethanol (≥99.8%, EtOH) were purchased from Carl Roth. 3-Aminopropyl triethoxysilane (98%, APTES) was purchased from ABCR. Tetraethyl ortho silicate (98%, TEOS) was purchased from Acros. Ethylene glycol- d_4 (EG- d_4 , deuteration degree of 98%) was obtained from Merck and used as obtained.

Synthesis of the Confinement Materials. Two porous silica materials were synthesized for use as confinement models

in this study, namely, pure SBA-15 (a) and SBA-15 functionalized with APTES (b). Both materials were synthesized by an optimized protocol based on the method described by Wang et al. 48 and Zeidan et al. 49 In a typical procedure, 21.3 g (0.017 equiv) of Pluronic P123 was dissolved in 573.7 mL (165 equiv) of deionized water, and 108.0 mL (6 equiv) of concentrated hydrochloric acid (37 wt %) was added. The solution was stirred for 48 h at 40 $^{\circ}$ C for preactivation.

Synthesis of Mesoporous Silica (SBA-15). 44.5 g portion (1 equiv) of TEOS was slowly dropped into the preactivated solution. A suspension was formed, which was stirred for another 24 h and transferred into a PTFE bottle. This suspension was aged under static conditions for 48 h at 90 °C. The precipitate was centrifuged, and the water was decanted. Then, the precipitate was resuspended in fresh solvent and centrifuged again. This procedure was repeated five times with deionized water and then one time with ethanol. The leftover template was removed by calcination. Before calcination, the crude product was dried at 90 °C and then calcined at 650 °C for 1 h with a heating rate of 5 K/min. Subsequently, the product was dried with a freeze-dryer. 6.5 g of SBA-15 were obtained.

Synthesis of APTES-Functionalized Mesoporous Silica (SBA-15 + APTES). 36.0 g (0.8 equiv) of TEOS was slowly dropped into the preactivated solution. 9.6 g (0.2 equiv) of APTES was added to this solution after 4 h. The suspension was stirred for another 24 h after the last addition and transferred to a PTFE bottle. The suspension was aged under static conditions for 48 h at 90 °C. The precipitate was centrifuged, and the water was decanted. Then, the precipitate was resuspended in fresh solvent and centrifuged again. This procedure was repeated five times with deionized water and then one time with ethanol. The removal of the template was performed by a Soxhlet extraction with ethanol for 48 h directly after the centrifugation procedure. Subsequently, the product was dried with a freeze-dryer. 9.9 g of APTES-functionalized SBA-15 was obtained.

Gas Adsorption Analysis. The characterization of the porosity and the specific surface area of the synthesized materials was performed by gas adsorption analysis at 77 K on a Thermo Fisher Scientific Surfer Brunauer-Emmett-Teller (BET) analyzer using nitrogen as an adsorbent. The adsorptiondesorption isotherms are shown in Supporting Information Figure S1. With the BET model, the specific surface area was calculated by analyzing the curve in the relative pressure (p/p_0) range between 0.02 and 0.35. Through the Gurvich method, at a p/p_0 value of 0.95, the pore volume was determined. By examining the adsorption–desorption isotherms in the p/p_0 range between 0.01 and 0.95 with the Barrett-Joyner-Halenda (BJH) method, the pore size distribution was obtained (Supporting Information Figure S2a). In addition, the pore size distribution was calculated by nonlocal density functional theory (NLDFT), employing cylindrical silica pores as a model for the calculation (Supporting Information Figure S2b).

Table 1 shows that the average pore diameters of both pure SBA-15 and SBA-15 modified with APTES are similar, which makes pure SBA-15 a suitable reference material. By combination of the data shown in Table 1 and the data obtained from elemental analysis (EA) shown in the Supporting Information, an APTES linker density of ca. 2.2 nm⁻² for the functionalized SBA-15 is calculated according to eq 1.

$$Linker\ density[nm^{-2}] = \frac{nitrogen\ loading\ [mol\cdot g^{-1}]}{specific\ surface\ area[m^2\cdot g^{-1}]} \cdot N_A \end{superinf}$$

Table 1. Specific Surface Area (BET), Pore Volume (Gurvich at p/p_0 =0.95), and Pore Diameter (BJH) for Each Synthesized Material^a

			pore diameter (d) [nm]		
sample	specific surface area (S) [m² g ⁻¹]	pore volume (V) $[\text{cm}^3 \text{g}^{-1}]$	вјн	NLDFT	average
SBA-15	714	0.89	5.7	7.0	6.4
SBA + APTES	537	0.72	5.5	7.9	6.7

^aThe averaged pore diameter is calculated from the pore diameters obtained with the BJH and the NLDFT method.⁵¹

where N_A is the Avogadro constant. According to Brodrecht et al.,⁵⁰ this linker density lets us assume that almost half of all available silanol groups are covered with APTES.

Sample Preparation. General: Both silica materials were pretreated under high vacuum (10^{-6} bar) at room temperature for 48 h and were transferred immediately to an argon-filled glovebox to avoid adsorption of atmospheric water. Under inert atmosphere conditions, samples of the pure SBA-15 (d=6.4 nm; S=714 m 2 g $^{-1}$; V=0.89 cm 3 g $^{-1}$) and the APTES-functionalized SBA-15 (d=6.7 nm; S=537 m 2 g $^{-1}$; V=0.72 cm 3 g $^{-1}$) were mixed with a volume of EG- d_4 corresponding to their respective pore volumes and left overnight to ensure absorption of the guest molecule inside the pores. The as-obtained samples 2 and 3, respectively, were stored in a glovebox before use.

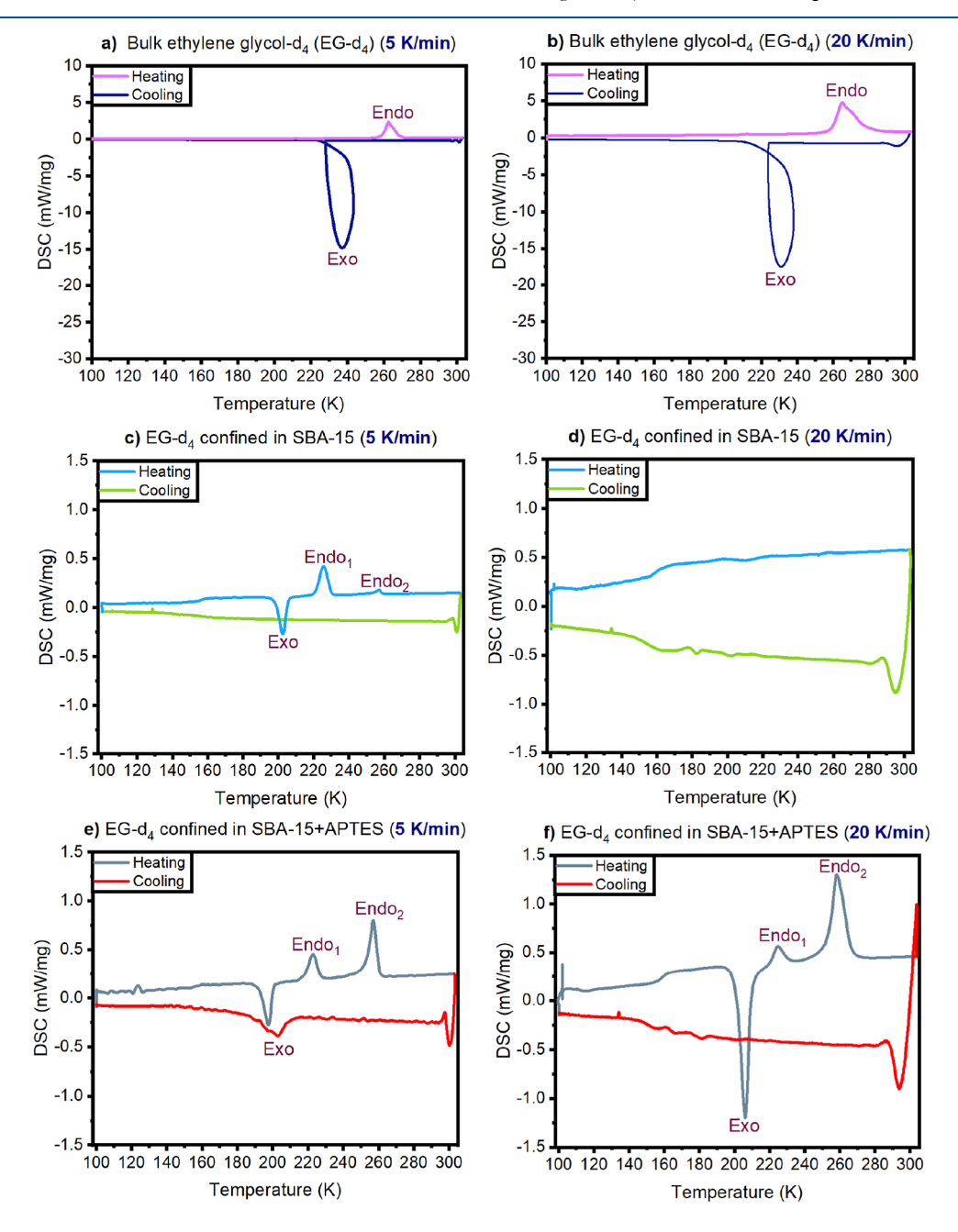


Figure 1. Experimental DSC curves for two heating/cooling rates on the left side: 5 K/min, and on the right side: 20 K/min. First row (a,b) belongs to the EG- d_4 in the bulk (sample 1), second (c,d) belongs to EG- d_4 confined in SBA-15 (sample 2), and third one (e,f) belongs to EG- d_4 confined in SBA-15 + APTES (sample 3). Note: Exo labels indicate the exothermic crystallization peak, and Endo₂ indicate endothermic melting peaks.

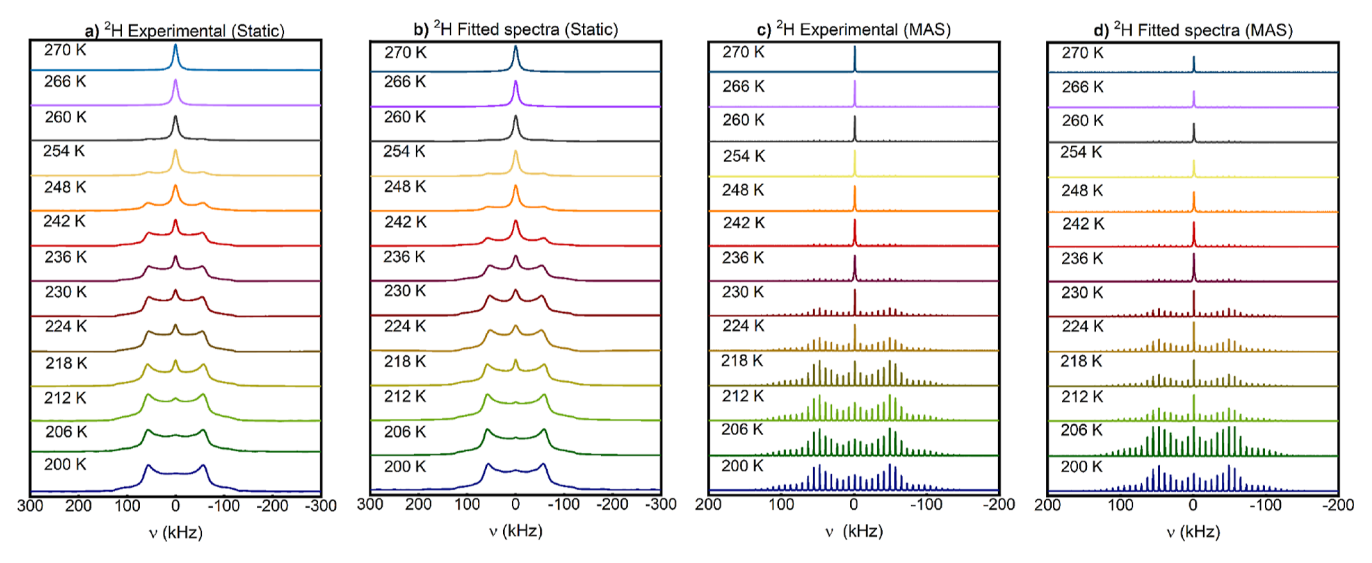


Figure 2. 2 H ssNMR spectra obtained in the temperature range between 200 and 270 K for EG- d_{4} in the bulk phase (sample 1). (a) 2 H static experimental data, (b) fitted 2 H static NMR spectra, (c) 2 H MAS experimental data, and (d) fitted 2 H MAS spectra.

DSC Samples. For DSC analysis, approximately 5 mg of each sample (1-3) were packed in aluminum crucibles and sealed with a sealing press.

²H NMR Samples. For ²H ssNMR measurements, approximately 20 mg of the as-prepared solid samples (2 and 3) were placed in 3.2 mm sapphire rotors, sealed by a PTFE plug, and closed with a ZrO_2 drive cap. In the case of EG- d_4 in the bulk phase (sample 1), 25 μL were filled into the rotor, and a silicon plug was fitted to close the rotor before the ZrO_2 drive cap was placed to avoid sample leaking.

Differential Scanning Calorimetry. DSC measurements were run on a NETZSCH 214 Polyma DSC. The samples for these experiments were prepared as described above and investigated in the temperature range between 100 and 300 K. The cooling and heating cycles were repeated three times. The heating/cooling rates used to carry out the different experiments were 5 7.5, 10, 15, 20, and 40 K/min. A temperature calibration with DSC standards (zink, indium, adamantane, cesium chloride, tin, and bismuth) was performed for each heating/ cooling rate. To exclude influences from the thermal history of the samples, only the second cooling and heating cycles were used for further analysis. Note that the data obtained in the third cycle were similar to the second run, while for the first run, deviations could be obtained. For more details on DSC experiments, the reader is referred to the Supporting Information.

Variable-Temperature ²H Solid-State NMR. All ²H ssNMR experiments at variable temperatures were carried out on a Bruker Avance III 400 MHz DNP NMR spectrometer equipped with a 9.4 T Ascend sweep-able magnet system corresponding to a frequency of 61.65 MHz for ²H and a 3.2 mm triple resonance ¹H/X/Y low-temperature MAS probe. The sample temperature was stabilized by a Bruker BioSpin low-temperature MAS cooling system. Spectra were acquired in the temperature range between 120 and 260 K. After each temperature set, a waiting period of 20 min was kept to stabilize the sample temperature. To confirm that NMR experiments were in thermal equilibrium at data acquisition independent of whether the final temperature was achieved by heating or cooling, exemplary spectra are compared in Supporting

Information Figure S5, showing identical spectra, which thus excludes hysteresis effects.

For temperature calibration, the approach described by Thurber and Tycko⁵² was utilized. The temperature readout from a thermocouple located close to the sample was used for the calibration data and subsequent experiments. For details, the reader is referred to the Supporting Information.

 2 H MAS NMR spectra were acquired with a single pulse sequence at a spinning rate of 8 kHz. A 2 μ s excitation pulse was used for all experiments, which corresponds to a flip angle of ca. 30° at 120 K. The recycle delay was set to 15 s. Each spectrum was recorded with 128 scans. Note that pulse optimization was performed with bulk EG- d_4 at 120 K.

 2 H static NMR experiments were carried out with the solid echo pulse sequence employing a pulse spacing of 40 μ s and pulses of 2 μ s length. The recycle delay was set to 15 s. Each spectrum was recorded with 1024 scans.

The static spectra were first fitted employing a laboratory-written MATLAB program described by some of the authors earlier ⁵³ and later analyzed employing the Roessler two-phase model. ⁵⁴ Fitting of ²H MAS spectra was performed with the DmFit2015 software package. ⁵⁵ To fit the MAS spectra shapes, a combination of two lines obtained with the Quad first model and the Gaussian/Lorentzian model, respectively, was used.

RESULTS

Monitoring of Thermodynamic Processes by DSC. Cooling and heating curves at scan rates of 5, 7.5, 10, 15, 20, and 40 K/min are shown for each sample in Figures S6–S8 in the Supporting Information. Figure 1 shows the most pertinent cooling and heating curves at scan rates of 5 and 20 K/min to illustrate the observed differences in the results between samples as well as scan rates. The cooling curves in Figure 1a,b of sample 1 (bulk EG- d_4) obtained at different scan rates both show an exothermic feature near 230 K. It is due to an instrumental artifact that this feature appears as a loop instead of a negative peak. ⁵⁶ The cause of this artifact is the rapid release of latent heat during the phase transition, outpacing the instrument's compensation capabilities. As a result, an artificially elevated temperature is recorded, diverging from the expected temperature according to the set cooling rate. The heating curves of

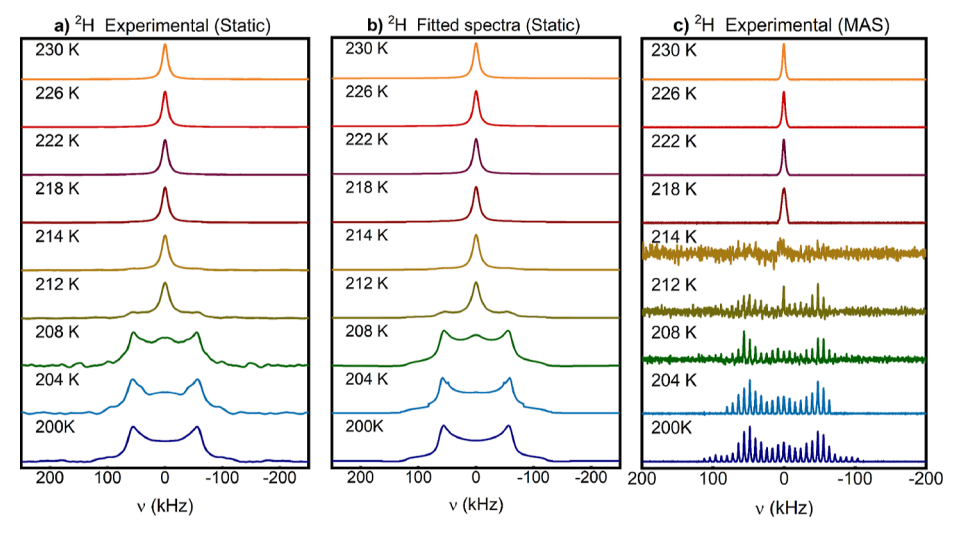


Figure 3. 2 H ssNMR spectra obtained in the temperature range between 200 and 230 K for EG- d_4 in SBA-15 (sample 2). (a) 2 H static NMR experimental data, (b) fitted 2 H static NMR spectra, and (c) 2 H MAS experimental data.

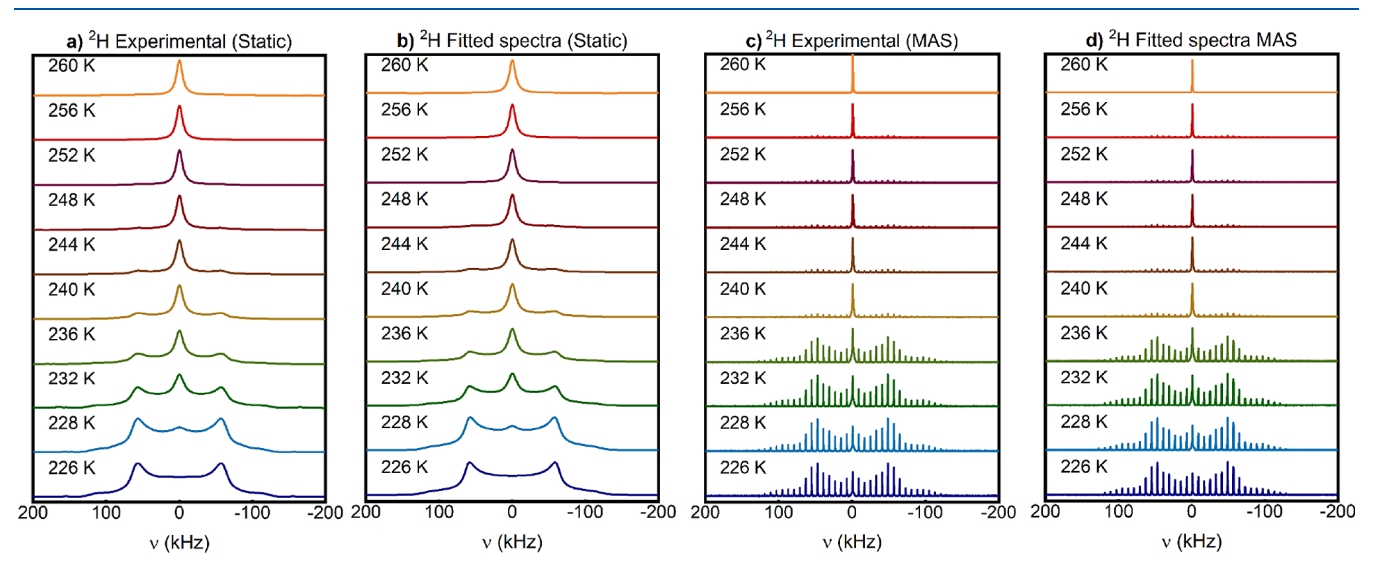


Figure 4. 2 H ssNMR spectra obtained in the temperature range between 226 and 260 K for EG- d_{4} in SBA- 15 + APTES (sample 3). (a) 2 H static experimental data, (b) fitted 2 H static NMR spectra, (c) 2 H MAS experimental data, and (d) fitted 2 H MAS spectra.

sample 1 in Figure 1a,b both display a single endothermic peak. The observed onset temperature is near $\sim\!264$ K, which is close to the reported melting temperature of bulk ethylene glycol $(261.6 \text{ K}).^{57}$ Owing to the width of the DSC peaks compared to the size of expected freezing point depressions, ⁵⁸ no attempts to perform a Gibbs—Thomson analysis were made.

Both cooling and heating curves in Figure 1c,d for sample 2 (EG- d_4 confined in SBA-15) show a small step-like feature near 155 K, which indicates the formation of a glass at temperatures below 155 K. Additional features are seen in the heating curve for sample 2 at heating rates lower than 10 K/min, as illustrated for 5 K/min in Figure 1c, where one exothermic peak slightly above 200 K and two endothermic peaks near 220 and 260 K are observed. These three features and the step-like feature are also observed at similar temperatures in the heating curves for sample 3 (EG- d_4 confined in SBA-15 + APTES) in Figure 1e,f, where the second endothermic peak is much more pronounced, as observed for sample 2. The cooling curves for sample 3 in Figure 1e,f also show a step-like feature near 155 K, but only clearly for the cooling rate of 20 K/min. For the cooling curve of 10 K/min

and lower, an exothermic peak is observed near 200 K, as can be seen as exemplary for 5 K/min in Figure 1e.

EG-d₄ Dynamics by Variable-Temperature ²H Solid-State NMR. ²H ss NMR spectra acquired under static and MAS conditions at temperature ranges where changes in the spectral line shape are discernible are shown for samples 1–3 in Figures 2–4, respectively. Also in the same figures, next to each set of acquired spectra, spectra simulated as described in the Experimental Section are included.

All spectra in Figures 2–4 display two features: a Pake pattern that dominates at low temperatures and a Lorentzian line that dominates at high temperatures. The temperature range during which the spectra change from Pake pattern dominant to Lorentzian line dominant varies from sample to sample, namely within 200–270 K for sample 1 (Figure 2), 200–230 K for sample 2 (Figure 3), and 226–260 K for sample 3 (Figure 4). There are no significant changes in the shape of the Pake pattern or the Lorentzian line in these spectra. Only their intensities change. The MAS spectra of sample 2 show a distorted line shape or a complete loss of signal in the temperature range

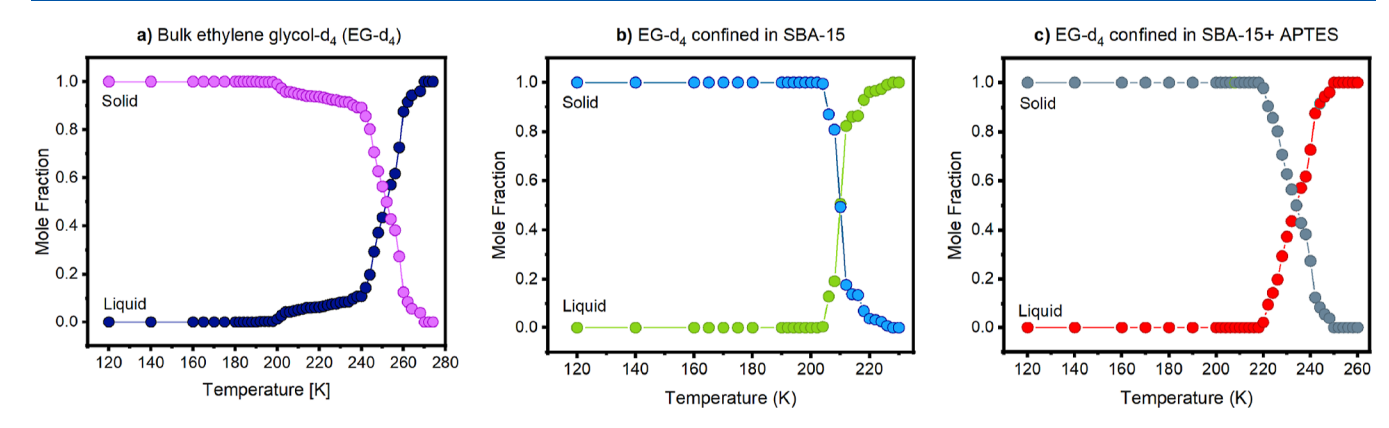


Figure 5. Change of fractions of the liquid-like and solid-like components during the phase transition, plotted as a function of temperature. The data points correspond to the relative areas of the liquid-like Lorentzian signal and the solid-like Pake pattern from the static 2 H NMR spectra measured under static conditions. (a) EG- d_4 in the bulk phase (sample 1), (b) EG- d_4 confined in SBA-15 (sample 2), and (c) EG- d_4 confined in SBA-15 + APTES (sample 3).

between 214 and 216 K. Thus, for sample 2, only the static spectra were fitted and presented in Figure 3. The reason why this special behavior is observed in the MAS spectra of sample 2 but not in the spectra obtained under static conditions lies in the stronger influence of relaxation on the MAS spectra, 59,60 which is discussed more in detail in Supporting Information Section 5. A detailed analysis of the spectral changes illustrated in Figures 2-4 is provided in Figure 5. This figure shows the fractions of the solid-like (Pake pattern) and liquid-like (Lorentzian line) components for the three investigated systems as a function of temperature. EG- d_4 in the bulk phase (Figure 5a) shows a slow, gradual transition within the temperature range of 208 and 240 K, followed by a faster transition from 240 to 266 K. In the case of EG-d₄ confined in SBA-15 (Figure 5b), a sharp step is obtained at 210 K, which covers only 10 K. For EG-d₄ confined in SBA-15 + APTES (Figure 5c), a smooth step is observed that starts near 220 K and completes near 256 K. The differences obtained for the three investigated systems are related to the interactions of the EG-d₄ molecules, which strongly depend on their chemical environments (bulk vs silica pore vs modified silica pore). A detailed analysis of our results is provided in the Discussion section.

DISCUSSION

The absence of a step-like feature in the cooling and heating curves of sample 1 in Figure 1a,b suggests that no glass is formed in sample 1. Instead, the observed exothermic and endothermic signals indicate freezing into a crystalline solid with subsequent melting. However, neat ethylene glycol has been described as an organic glass-former that undergoes structural relaxation processes below its glass transition temperature, ³⁸ resulting in a complex coexistence of glassy and crystalline phases. This might explain why the ssNMR spectral changes in Figure 2 for sample 1 occur over a much wider temperature range than the temperature where the exo- and endothermic features are observed in Figure 1a,b. ssNMR is sensitive to changes in motion, which may occur well below the phase transition temperature. 61 In this regard, it is important to keep in mind that the ssNMR spectra in Figures 2-4 were reproducible, regardless if they were obtained from cooling or heating the samples (see Experimental Section and Figure S5 in the Supporting Information). The range of temperatures for which ssNMR spectral changes are observed for sample 3 in Figure 4 matches well the range of temperatures over which the two endothermic peaks are observed in the heating curves of sample 3 in Figure 1e,f. However, the ssNMR spectral changes are monotonous and are not in steps. Thus, motional changes occur gradually in contrast to the distinct phase changes indicated by the separate endothermic peaks in Figure 1e,f. The ssNMR spectral changes for sample 2 in Figure 3 appear to be complete at 230 K, i.e., over a narrower range of temperatures than those for samples 1 and 3. However, the endothermic peak "Endo₂" is only weekly present in Figure 1c,d, and the fraction of molecules associated with this phase transition might have been too small to detect their changes in motion in the ssNMR spectrum. The temperature of 230 K does indeed match well with the temperature at which the phase transition associated with the endothermic peak "Endo₁" in Figure 1c,d is complete.

For a deeper analysis of molecular dynamics in the three investigated systems, the quadrupolar coupling constants ($C_{\rm Q}$), obtained from the line shape simulation of the static and MAS spectra, were plotted as a function of temperature in Figure 6. Recalling that $C_{\rm Q}$ serves as a sensitive indicator, enabling us to observe alterations in nuclear positions and their local environments.

As shown in Figure 6, for MAS as well as for static experiments, in the low temperature range, a maximum value of $C_0 \approx 168$ kHz for the 3 samples is obtained, which is typical

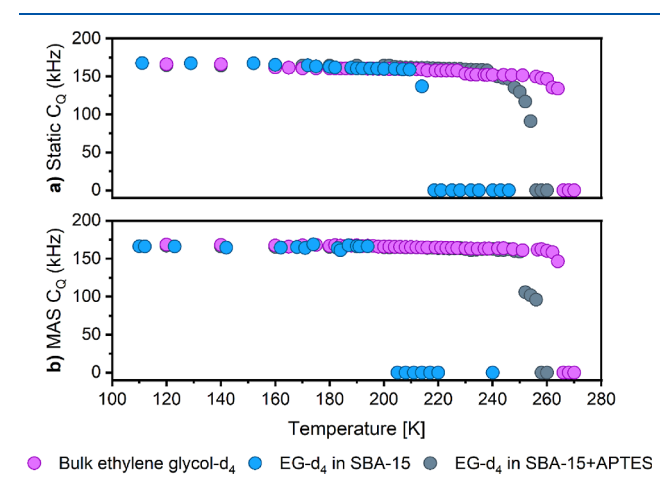


Figure 6. Values of the quadrupolar coupling constants (C_Q) extracted from the simulated spectra as a function of temperature: (a) 2H static NMR spectra and (b) 2H MAS spectra.

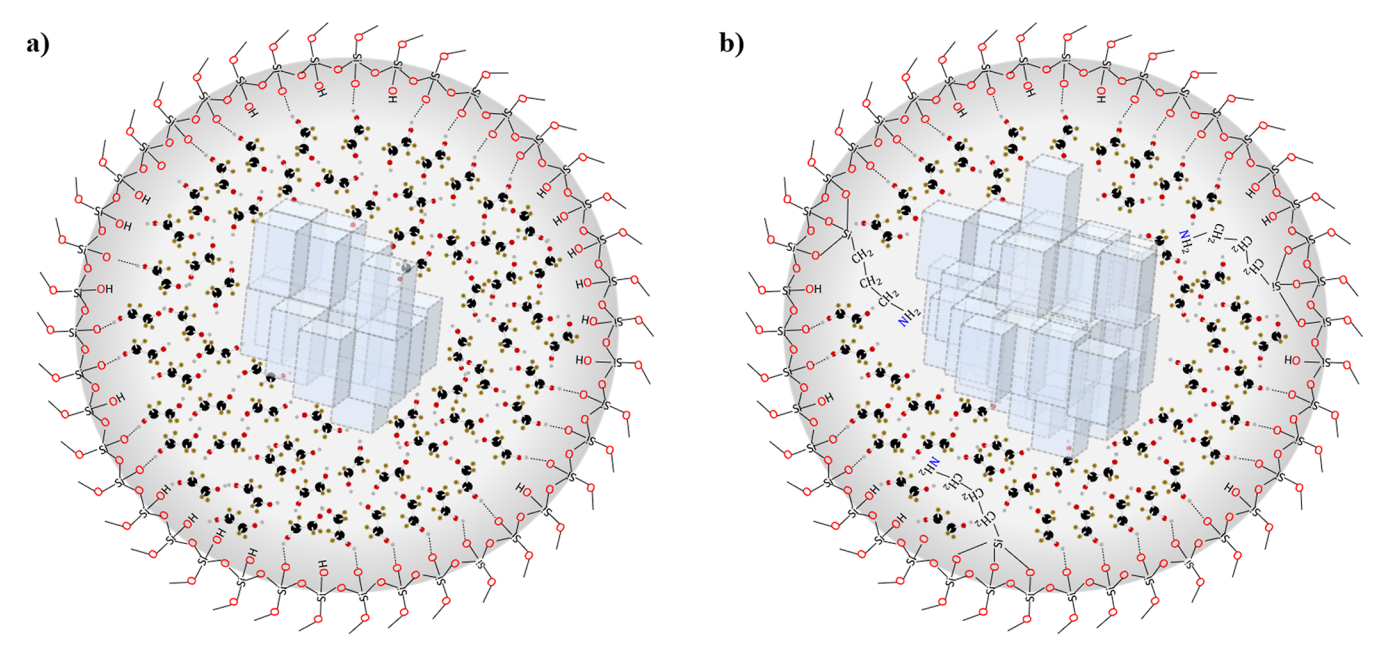


Figure 7. Schematic illustration of the arrangement of EG- d_4 molecules inside the pores of (a) pure SBA-15 and (b) APTES-functionalized SBA-15. This picture includes the formation of crystal-like structures of EG- d_4 in the middle of the pores as well as amorphous structures of EG- d_4 close to the pore wall.

for rigid or slow motional CD bonds. At low temperatures, EG- d_4 undergoes slow motions on a negligible time scale; therefore, the line shape of the spectra is unaffected for the 3 samples. When the mobility of the molecule increases and motional averaging occurs, a reduction in the time-averaged quadrupolar interaction takes place, which causes the value of $C_{\rm Q}$ to decrease.

The fact that the shape of the Pake pattern is essentially temperature-independent as well as identical for all three samples suggests that the deuterium nuclei experience the same electric field gradient when ethylene glycol is in the solid phase, confined, or unconfined. There are two possibilities that cannot be differentiated based on the ssNMR data alone: (a) the solid phase is exclusively a crystalline solid for all three samples, and (b) the electric field gradient experienced by the $-CD_2$ deuterium atoms is the same, regardless if the solid phase is crystalline or in a glass state. The fact that the ssNMR showed no hysteresis effects (cooling vs heating) suggests that the samples were at thermodynamic equilibrium, which should be the crystalline phase, and thus suggests that the former scenario applies. However, the fact that even at the lowest scan rate of 5 K/min the formation of a glass phase is indicated in the DSC data for sample 2 in Figure 1c,d suggests that the latter scenario applies. The latter scenario is also supported by the T_2 relaxation data for sample 2 in Figure S11 in the SI. The continual drop in T_2 that is completed just below 200 K coincides well with the exothermic peak in the heating curve of sample 2 in Figure 1c,d. This suggests that sample 2 underwent a transition from a glass to a crystalline solid, to which the ssNMR spectra in Figure 3 were completely oblivious as they show the exact same Pake pattern for all temperatures below 200 K.

The two endothermic peaks in the heating curve of confined ethylene glycol in Figure 1 were also reported by Reuhl et al. ³³ for some of their samples in their study of ethylene glycol confined in silica pores of varying pore size. In that study, the DSC samples consisted of silica pore material impregnated with excess ethylene glycol, and the Endo₂ peak was assigned to the melting of frozen excess ethylene glycol outside of the pores.

The temperature at which they obtained the Endo2 peak matches well with the endothermic peak in the heating curve of sample 1 in Figure 1 (~265 K). The Endo₁ peak was assigned to the occurrence of a liquid phase inside the pore, which was further corroborated by T_1 relaxation and NMR self-diffusion measurements. These showed that at temperatures between the two endo peaks, a coexistence of a liquid and solid phase was present in the pores. The ssNMR spectra in Figures 3 and 4 confirm this assignment because the observation of a spectral component with Lorentzian shape indicates that some parts of the ethylene glycol molecule can tumble freely. The preparation procedures for samples 2 and 3 are intended to avoid overfilling, and capillary forces should result in complete absorption of the impregnating liquid. While it is principally possible that not all ethylene glycol was absorbed, this cannot be the sole explanation for at least the Endo₂ peak in Figure 1e,f for sample 3. Here, the endo peak is more than twice as large as the Endo, peak, implying that more than 2/3 of the ethylene glycol was outside of the pore, which is very unlikely. Given the just-mentioned evidence for the coexistence of solid and liquid ethylene glycol inside the pore provided by the study by Reuhl, 33 we assume that a portion of the confined ethylene glycol, situated at the center of the pore, remains in the solid state at low temperatures. Although this location does not completely cancel the influence of the pore walls on the confined molecules, it does prevent EGd₄ in that position from adopting a glassy structure at low temperatures. Under these assumptions, it appears more likely that the Endo, peak arises from the melting of a fraction of the confined ethylene glycol situated within the core of the pore, while the Endo₂ peak is in large part, if not solely, due to the melting of the remaining solid ethylene glycol inside the pore. Compared to sample 2, the APTES surface decoration in sample 3 leads to a substantially larger portion of ethylene glycol in the pore that remains solid after the first melting event upon heating the sample, as schematically depicted in Figure 7. This effect of APTES can be rationalized in terms of the intermolecular interactions of ethylene glycol on the pore surface. These

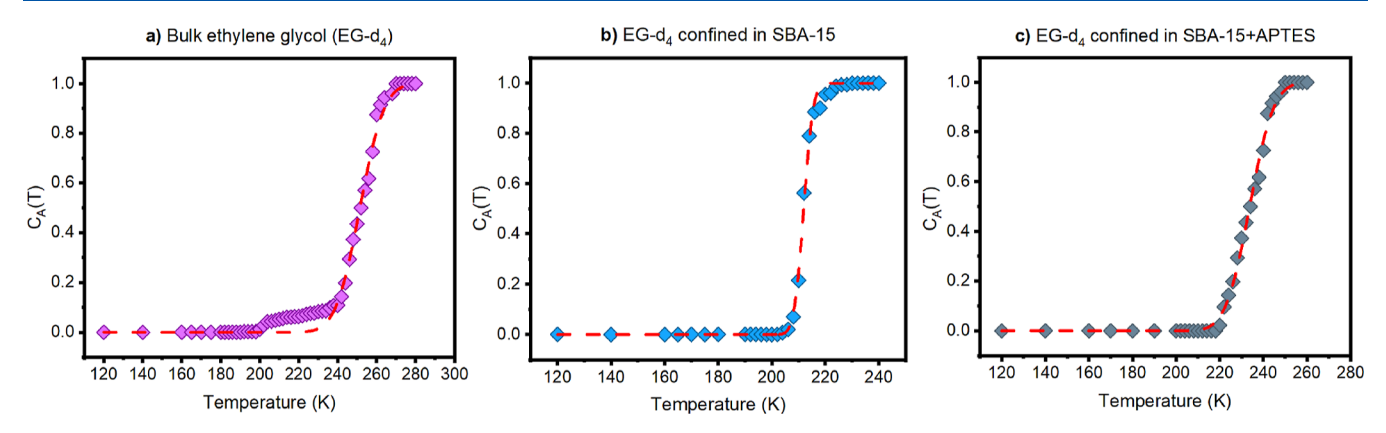


Figure 8. Mole fraction of the fast-moving component in the samples as a function of temperature, including the fitting with eq 2.

interactions are anticipated to be more pronounced with the silanol surface compared with the APTES-decorated surface. This difference can be attributed to the lower polarity of APTES and its reduced capacity to participate in hydrogen bonding in contrast to silanol surface groups, which can both accept and donate protons for hydrogen bonding. 62 Strong interactions of ethylene glycol with the pore surface are supported by the reported slowed ethylene glycol dynamics. 33 Strong interactions with the pore surface should disrupt the intermolecular interactions between the ethylene glycol molecules. As a result of these disruptions, the tendency of EG-d₄ to undergo crystalline solid formation is diminished. Conversely, the preferential interactions with the pore surface relative to neighboring molecules allow for a breakup of the crystalline structure at lower temperatures than in the bulk. Thus, the ethylene glycol molecules near the pore surface melt first upon heating, and the glycol molecules sufficiently distanced from the pore surface behave similar to bulk ethylene glycol and stay solid until the bulk melting temperature is reached. For sample 2 without the APTES surface modification, this fraction of ethylene glycol molecules is rather small (Figure 7a), while for sample 3 with the APTES modification and an otherwise similar average pore size, this fraction of molecules is much larger because the weaker interactions of ethylene glycol with the APTES affect a smaller number of layers of ethylene glycol molecules adjacent to the pore surface (Figure 7b). This molecular interpretation is corroborated by the absence of the Endo1 peak for silica material of very small average pore sizes, as reported by Reuhl et al.33

Interestingly, the intensity of the Lorentzian line-shape component in Figures 2-5 gradually increases with increasing temperature and not in discrete increments as one might expect from the presence of the two separate endothermic peaks in the heating curves. This suggests that the underlying isotropic motions of ethylene glycol are present even for some of the ethylene glycol molecules that are solid within the pore. One possible explanation is that freezing and melting processes are highly dynamic at the molecular level. A molecule that is freely tumbling may lose the necessary kinetic energy to a neighboring molecule and stop tumbling, while the neighboring molecule now tumbles freely. With increasing temperature, the frequency of intermolecular energy transfer may increase and involve an increasing number of molecules, so that the Pake pattern gradually decreases in the ssNMR spectra while the contribution of the Lorentzian line increases. As already pointed out, the temperatures at which the Lorentzian line dominates the ssNMR match well with the temperature at which the Endo peak is observed in the respective heating curves, which would imply that at this temperature molecules remain tumbling freely, thus requiring an increase in free energy. Such a motional process would be random in nature, with varying correlation times for staying in a state of freely tumbling.⁵³

Rössler et al. 63 proposed a method to determine the distribution of activation energies for guest molecules in polymer systems, which was later adapted by some of us to molecules in porous systems. 19,44,54,64,65 The dynamics of confined molecules, here partially deuterated ethylene glycol, are divided into two groups, one with a fast jump regime (liquid-like) and the other with a slow jump regime (solid-like). This model excludes any intermediate jump mechanism. eq 2 shows the temperature dependence of what Rössler referred to as the relative intensity of the fast-jumping component, $C_{\rm A}(T)$. In essence, though $C_{\rm A}(T)$ may simply be thought of as the mole fraction of the fast-jumping component, we will continue to use the phrase mole fraction for clarity.

$$C_{\mathbf{A}}(T) = \int_0^T \frac{1}{\sqrt{2\pi\Delta T^2}} \exp\left(-\frac{(T - T_0)^2}{2\Delta T^2}\right) dT$$
$$= \frac{1}{2} \operatorname{erf}\left(\frac{1}{\sqrt{2\Delta T}}(T - T_0)\right) + \frac{1}{2} \operatorname{erf}\left(\frac{1}{\sqrt{2\Delta T}}T_0\right)$$
(2)

where erf (x) is the Gaussian error function, which is close to 0 at low temperatures and close to 1 at high temperatures, T_0 is the melting point as the center of gravity, and ΔT is the width of the distribution.

From eq 2, the distribution of the activation energies g(E) in temperature units is obtained by eq 3 as follows.

$$g(E) = \frac{\mathrm{d}}{\mathrm{d}T}C_{\mathrm{A}} = \frac{1}{\sqrt{2\pi\Delta T}} \exp\left(-\frac{(T-T_0)^2}{2\Delta T^2}\right) \tag{3}$$

Figure 8a–c shows the experimental C_A values as a function of temperature T (diamonds) in comparison with $C_A(T)$ obtained from eq 2 (red dashed line) for the three investigated samples. It is shown in Figure 8a that the model does not fit properly for the EG- d_4 in the bulk phase (sample 1). As is visible in the temperature range between 200 and 240 K, deviations from experimental data are obtained. This deviation is attributed to the onset of dynamics for a portion of molecules in this temperature range, which is not included in the fit model. For EG- d_4 in confined environment (samples 2 and 3) (Figure 8b,c), the employed two-phase model suitably describes the experimental results, which suggests that NMR spectra capture

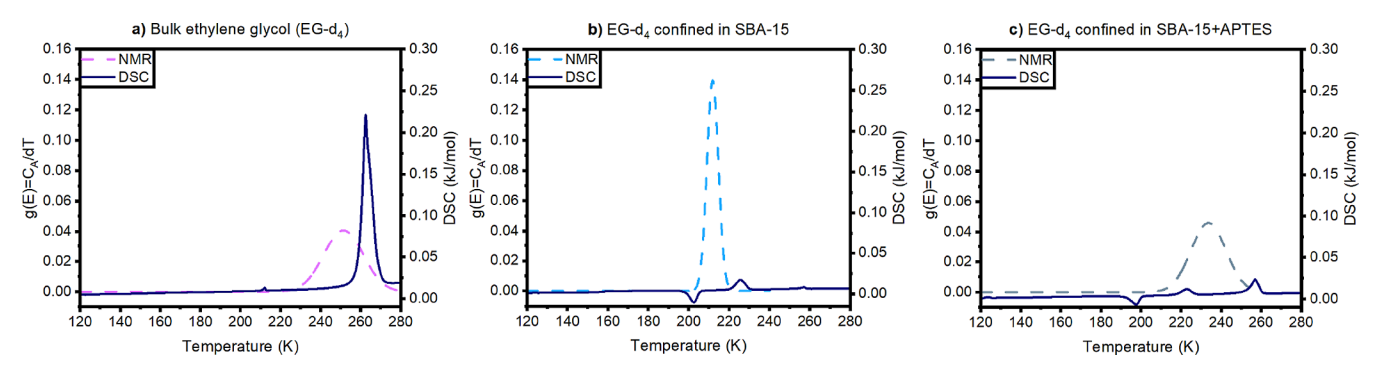


Figure 9. Comparison of activation energy distributions obtained from the NMR spectra caused by isotropic motions and the DSC curves encoding translational motions of EG- d_4 as a function of temperature for (a) EG- d_4 in the bulk phase (sample 1), (b) EG- d_4 confined in SBA-15 (sample 2), and (c) EG- d_4 confined in SBA-15 + APTES (sample 3). The distributions of activation energies (dashed lines) were calculated with eq 3. The DSC curves (solid lines) were recorded at 5 K/min.

ı

two types of molecular motions: the fast motions (liquid-like), attributed to molecules mainly located in close vicinity of the pore wall, and the comparably slow-frequency motions, caused by the molecules in the center of the pore (solid-like). With increasing temperature, the number of molecules that contribute to the Lorentzian component (liquid-like) increases until all of them reach the state of melting.

A comparison between the activation energy distributions encoding isotropic motions in EG- d_4 and the DSC curves encoding translational motions of EG-d₄ obtained during heating is shown in Figure 9 for the three investigated systems. For EG- d_4 in the bulk (Figure 9a), the energy distribution g(E) shows a maximum at 252 K, which is 11 K lower than the phase transition obtained in the DSC curve at 263 K. For EG-d₄ confined in SBA-15 (Figure 9b), the distribution of activation energies reaches its maximum at 212 K, which is 14 K lower than the first melting event at 226 and 45 K lower than the second melting event at 257 K. Finally, in the case of EG- d_4 confined in SBA-15 + APTES (Figure 9c), the maximum of the activation energy distribution is obtained at 234 K, 11 K higher than the first melting event at 223 and 23 K lower than the second melting event at 257 K. The distribution of activation energies g(E) for EG- d_4 in the bulk (sample 1) and EG- d_4 confined in SBA-15 + APTES (sample 3) contain similar widths with ΔT ~ 30 K but with a center of gravity T_0 that is ${\sim}18$ K higher for sample 1 compared to sample 3. In contrast, the distribution for EG- d_4 in SBA-15 (sample 2) is significantly narrower compared to the activation energy distributions for samples 1 and 3.

The phase transitions obtained in the DSC curves refer to a change in the translational motion of EG- d_4 . For the confined samples, several phase transitions are observed all along the heating phase. According to the NMR results, the isotropic motions are, however, not affected during the phase transitions. The narrower distribution of the activation energy in sample 2 can be explained by the large amount of EG- d_4 distributed in the vicinity of the pore wall. The large number of hydrogen bonds established between the guest molecules and the immobile hydroxyl groups of the pore walls lead EG-d₄ molecules to adopt a glassy state behavior, including faster dynamics when increasing temperature in comparison with samples 1 and 3.66 This amount is significantly lower for sample 3, where a significant part of the surface hydroxy groups has been reacted with the ethoxy groups of the APTES, and other parts might be inaccessible due to blocking by the APTES alkyl chain.

CONCLUSIONS

In this study, the influence of APTES groups at the pore walls of SBA-15 on the dynamics of deuterated ethylene glycol (EG- d_4) was inspected by comparing three systems, namely EG-d₄ confined in APTES functionalized SBA-15 (sample 1), EG-d₄ confined in SBA- 15 (sample 2) and EG- d_4 in the bulk phase (sample 3). By differential scanning calorimetry (DSC) analysis, significant differences in the physical properties (melting, crystallization, glass formation, etc.) are obtained for the three systems. In confinement, the molecules experience different interactions, namely (i) in the vicinity of the pore wall, (ii) in the pore center, and (iii) in an intermediate region between them. Hydrogen bonds formed between the silanol groups at the pore walls and the EG- d_4 have a strong impact on the alignment of EG- d_4 , which does not allow them to form ordered crystal-like structures. This impact decreases as more molecules are joined by hydrogen bonds between EG- d_4 molecules. The presence of APTES groups reduces the level of hydrogen bond formation between EG- d_4 molecules and the pore wall. The decrease of O...HO hydrogen bonds between EG-d₄ molecules and OH groups at the pore wall results in an increased number of EG- d_4 molecules in the center of the pore that adopt dynamics comparable to bulk EG- d_4 . This is contrary to EG- d_4 molecules in pure SBA- 15, where, due to these hydrogen bonds, glass transitions are dominant.

Through line shape analysis of the $^2\mathrm{H}$ solid-state NMR spectra at variable temperatures, two components were identified at temperatures where the phase transition takes place: (i) Lorentzian lines, representative for a liquid-like phase, and (ii) a Pake pattern, representative for a solid-like phase. Employing the two-phase model proposed by Rössler, the distribution of activation energies of the tree systems was calculated. The similar broad distributions of activation energies calculated for EG- d_4 in APTES-modified SBA-15 and EG- d_4 in the bulk phase indicate similarities in the dynamics in the two systems. On the contrary, for EG- d_4 confined in pure SBA-15, a narrower activation energy distribution is obtained, which underlines the strong influence of O···HO hydrogen bond formation between EG- d_4 and OH groups at the surface of SBA-15 on the EG- d_4 dynamics.

In summary, our findings on interactions of EG- d_4 with APTES-decorated SBA-15 will help in the future to better understand the role of confinement in drug delivery systems as well as to understand heterogeneously catalyzed reactions in green solvents. Moreover, they can serve as an experimental database for molecular dynamics simulations of confined EG.

ASSOCIATED CONTENT

Supporting Information

The Supporting Information is available free of charge at https://pubs.acs.org/doi/10.1021/acs.jpcc.3c03671.

Characterization of the pore of both materials, protocol for the analysis of DSC performed in this study, temperature calibration protocol as well as temperature variation, DSC results for each of the samples, and explanation of the lack of signal from sample 2 (PDF)

AUTHOR INFORMATION

Corresponding Authors

Torsten Gutmann — Eduard-Zintl-Institut für Anorganische und Physikalische Chemie, Technische Universität Darmstadt, Darmstadt D-64287, Germany; ⊙ orcid.org/0000-0001-6214-2272; Email: gutmann@chemie.tu-darmstadt.de

Gerd Buntkowsky — Eduard-Zintl-Institut für Anorganische und Physikalische Chemie, Technische Universität Darmstadt, Darmstadt D-64287, Germany; oorcid.org/0000-0003-1304-9762; Email: gerd.buntkowsky@chemie.tudarmstadt.de

Authors

Nadia B. Haro Mares — Eduard-Zintl-Institut für Anorganische und Physikalische Chemie, Technische Universität Darmstadt, Darmstadt D-64287, Germany

Martin Brodrecht — Eduard-Zintl-Institut für Anorganische und Physikalische Chemie, Technische Universität Darmstadt, Darmstadt D-64287, Germany

Till Wissel – Eduard-Zintl-Institut für Anorganische und Physikalische Chemie, Technische Universität Darmstadt, Darmstadt D-64287, Germany

Sonja C. Döller – Eduard-Zintl-Institut für Anorganische und Physikalische Chemie, Technische Universität Darmstadt, Darmstadt D-64287, Germany

Lorenz Rösler – Eduard-Zintl-Institut für Anorganische und Physikalische Chemie, Technische Universität Darmstadt, Darmstadt D-64287, Germany; orcid.org/0000-0002-0742-7969

Hergen Breitzke – Eduard-Zintl-Institut für Anorganische und Physikalische Chemie, Technische Universität Darmstadt, Darmstadt D-64287, Germany

Markus M. Hoffmann – Department of Chemistry and Biochemistry, State University of New York at Brockport, Brockport, New York 14420, United States; ⊙ orcid.org/ 0000-0002-5469-8665

Complete contact information is available at: https://pubs.acs.org/10.1021/acs.jpcc.3c03671

Notes

The authors declare no competing financial interest.

ACKNOWLEDGMENTS

Financial support by the Deutsche Forschungsgemeinschaft under contract Bu-911-24-3 and by the National Science Foundation under grant no. 1953428 is gratefully acknowledged.

REFERENCES

(1) Calvillo, L.; Celorrio, V.; Moliner, R.; Cabot, P. L.; Esparbé, I.; Lázaro, M. Control of textural properties of ordered mesoporous materials. *Microporous Mesoporous Mater.* **2008**, *116* (1–3), 292–298.

- (2) Amitay-Rosen, T.; Vega, S. A deuterium MAS NMR study of the local mobility of dissolved methionine and di-alanine at the inner surface of SBA-15. *Phys. Chem. Chem. Phys.* **2010**, 12 (25), 6763–6773.
- (3) Ciesla, U.; Schüth, F. Ordered mesoporous materials. *Microporous Mesoporous Mater.* **1999**, 27 (2–3), 131–149.
- (4) Li, Y.; Shi, J. Hollow-structured mesoporous materials: chemical synthesis, functionalization and applications. *Adv. Mater.* **2014**, *26* (20), 3176–3205.
- (5) Wang, L.; Ding, W.; Sun, Y. The preparation and application of mesoporous materials for energy storage. *Mater. Res. Bull.* **2016**, *83*, 230–249.
- (6) Schüth, F.; Schmidt, W. Microporous and Mesoporous Materials. *Adv. Mater.* **2002**, *14* (9), 629–638.
- (7) Moritz, M.; Geszke-Moritz, M. Mesoporous materials as multifunctional tools in biosciences: principles and applications. *Mater. Sci. Eng.*, C 2015, 49, 114–151.
- (8) Zhao, D.; Feng, J.; Huo, Q.; Melosh, N.; Fredrickson, G. H.; Chmelka, B. F.; Stucky, G. D. Triblock copolymer syntheses of mesoporous silica with periodic 50 to 300 angstrom pores. *Science* **1998**, 279 (5350), 548–552.
- (9) Sing, K. S. W. Reporting physisorption data for gas/solid systems with special reference to the determination of surface area and porosity (Recommendations 1984). *Pure Appl. Chem.* **1985**, *57* (4), 603–619.
- (10) Brodrecht, M.; Kumari, B.; Thankamony, A. S. S. L.; Breitzke, H.; Gutmann, T.; Buntkowsky, G. Structural Insights into Peptides Bound to the Surface of Silica Nanopores. *Chem.—Eur. J.* **2019**, 25 (20), 5214–5221.
- (11) Rodríguez-de-la-Peña, S.; Gómez-Salazar, S.; Gutiérrez-Ortega, J. A.; Badillo-Camacho, J.; Peregrina-Lucano, A. A.; Shenderovich, I. G.; Manríquez-González, R. Novel Silica Hybrid Adsorbent Functionalized with l-Glutathione Used for the Uptake of As(V) from Aqueous Media. *Ind. Eng. Chem. Res.* **2022**, *61* (12), 4348–4362.
- (12) Gutiérrez-Ortega, J. A.; Gómez-Salazar, S.; Shenderovich, I. G.; Manríquez-González, R. Efficiency and lead uptake mechanism of a phosphonate functionalized mesoporous silica through P/Pb association ratio. *Mater. Chem. Phys.* **2020**, 239, 122037.
- (13) Liu, Y.; Liao, J.; Chang, L.; Bao, W. Ag modification of SBA-15 and MCM-41 mesoporous materials as sorbents of thiophene. *J. Fuel* **2022**, 311, 122537.
- (14) Brodrecht, M.; Breitzke, H.; Gutmann, T.; Buntkowsky, G. Biofunctionalization of Nano Channels by Direct In-Pore Solid-Phase Peptide Synthesis. *Chem.—Eur. J.* **2018**, *24* (*67*), 17814–17822.
- (15) Alothman, Z. A Review: Fundamental Aspects of Silicate Mesoporous Materials. *Materials* **2012**, *5* (12), 2874–2902.
- (16) Putz, A.-M.; Almásy, L.; Len, A.; Ianăşi, C. Functionalized silica materials synthesized via co-condensation and post-grafting methods. *Fullerenes, Nanotub. Carbon Nanostruct.* **2019**, 27 (4), 323–332.
- (17) Brodrecht, M.; Kumari, B.; Breitzke, H.; Gutmann, T.; Buntkowsky, G. Chemically Modified Silica Materials as Model Systems for the Characterization of Water-Surface Interactions. *Z. Phys. Chem.* **2018**, 232 (7–8), 1127–1146.
- (18) Thompson, W. H. Perspective: Dynamics of confined liquids. *J. Chem. Phys.* **2018**, *149* (17), 170901.
- (19) Gedat, E.; Schreiber, A.; Albrecht, J.; Emmler, T.; Shenderovich, I.; Findenegg, G. H.; Limbach, H.-H.; Buntkowsky, G. 2 H-Solid-State NMR Study of Benzene- d6 Confined in Mesoporous Silica SBA-15. *J. Phys. Chem. B* **2002**, *106* (8), 1977–1984.
- (20) Wang, G.; Otuonye, A. N.; Blair, E. A.; Denton, K.; Tao, Z.; Asefa, T. Functionalized mesoporous materials for adsorption and release of different drug molecules: A comparative study. *J. Solid State Chem.* **2009**, *182* (7), 1649–1660.
- (21) Jiang, S.; Yu, D.; Ji, X.; An, L.; Jiang, B. Confined crystallization behavior of PEO in silica networks. *Polymer* **2000**, *41* (6), 2041–2046. (22) Korb, J.-P.; Xu, S.; Jonas, J. Confinement effects on dipolar

relaxation by translational dynamics of liquids in porous silica glasses. *J. Chem. Phys.* **1993**, *98* (3), 2411–2422.

(23) Koone, N.; Shao, Y.; Zerda, T. W. Diffusion of Simple Liquids in Porous Sol-Gel Glass. *J. Phys. Chem.* **1995**, *99* (46), 16976–16981.

- (24) Zhang, J.; Liu, G.; Jonas, J. Effects of confinement on the glass transition temperature of molecular liquids. *J. Phys. Chem.* **1992**, *96* (8), 3478–3480.
- (25) Buntkowsky, G.; Vogel, M. Small Molecules, Non-Covalent Interactions, and Confinement. *Molecules* **2020**, 25 (14), 3311.
- (26) Otalvaro, J. O.; Avena, M.; Brigante, M. Adsorption of organic pollutants by amine functionalized mesoporous silica in aqueous solution. Effects of pH, ionic strength and some consequences of APTES stability. *J. Environ. Chem. Eng.* **2019**, 7 (5), 103325.
- (27) Bruce, I. J.; Sen, T. Surface modification of magnetic nanoparticles with alkoxysilanes and their application in magnetic bioseparations. *Langmuir* **2005**, *21* (15), 7029–7035.
- (28) Rahman, I. A.; Jafarzadeh, M.; Sipaut, C. S. Synthesis of organo-functionalized nanosilica via a co-condensation modification using γ -aminopropyltriethoxysilane (APTES). *Ceram. Int.* **2009**, 35 (5), 1883–1888.
- (29) de Oliveira, M.; Herr, K.; Brodrecht, M.; Haro-Mares, N. B.; Wissel, T.; Klimavicius, V.; Breitzke, H.; Gutmann, T.; Buntkowsky, G. Solvent-free dynamic nuclear polarization enhancements in organically modified mesoporous silica. *Phys. Chem. Chem. Phys.* **2021**, 23 (22), 12559–12568.
- (30) Maria Chong, A. S.; Zhao, X. S. Functionalization of SBA-15 with APTES and Characterization of Functionalized Materials. *J. Phys. Chem. B* **2003**, *107* (46), 12650–12657.
- (31) Crupi, V.; Magazù, S.; Majolino, D.; Migliardo, P.; Bellissent-Funel, M. Dynamical study of confined ethylene glycol by IQENS. *Physica B* **2000**, 276–278, 417–418.
- (32) Narayan, R.; Nayak, U. Y.; Raichur, A. M.; Garg, S. Mesoporous Silica Nanoparticles: A Comprehensive Review on Synthesis and Recent Advances. *Pharmaceutics* **2018**, *10* (3), 118.
- (33) Reuhl, M.; Weigler, M.; Brodrecht, M.; Buntkowsky, G.; Vogel, M. Nuclear Magnetic Resonance and Broadband Dielectric Spectroscopy Studies on the Dynamics of Ethylene Glycol in Mesoporous Silica. *J. Phys. Chem. C* **2020**, *124* (38), 20998–21012.
- (34) Czaderna-Lekka, A.; Kozanecki, M.; Matusiak, M.; Kadlubowski, S. Phase transitions of poly(oligo(ethylene glycol) methyl ether methacrylate)-water systems. *Polymer* **2021**, *212*, 123247.
- (35) Jiang, Y.-Q.; Li, J.; Feng, Z.-W.; Xu, G.-Q.; Shi, X.; Ding, Q.-J.; Li, W.; Ma, C.-H.; Yu, B. Ethylene Glycol: A Green Solvent for Visible Light-Promoted Aerobic Transition Metal-Free Cascade Sulfonation/Cyclization Reaction. *Adv. Synth. Catal.* **2020**, *362* (13), 2609–2614.
- (36) Yue, H.; Zhao, Y.; Ma, X.; Gong, J. Ethylene glycol: properties, synthesis, and applications. *Chem. Soc. Rev.* **2012**, *41* (11), 4218–4244.
- (37) Buntkowsky, G.; Döller, S.; Haro-Mares, N.; Gutmann, T.; Hoffmann, M. Solid-state NMR studies of non-ionic surfactants confined in mesoporous silica. *Z. Phys. Chem.* **2022**, 236 (6–8), 939–960.
- (38) Gao, C.; Zhou, G.-Y.; Xu, Y.; Hua, T.-C. Glass transition and enthalpy relaxation of ethylene glycol and its aqueous solution. *Thermochim. Acta* **2005**, *4*35 (1), 38–43.
- (39) Döller, S. C.; Brodrecht, M.; Haro Mares, N. B.; Breitzke, H.; Gutmann, T.; Hoffmann, M.; Buntkowsky, G. Deuterium NMR Studies of the Solid-Liquid Phase Transition of Octanol- d17 Confined in SBA-15. *J. Phys. Chem. C* **2021**, *125* (45), 25155–25164.
- (40) Zheng, Q.; Zhang, Y.; Montazerian, M.; Gulbiten, O.; Mauro, J. C.; Zanotto, E. D.; Yue, Y. Understanding Glass through Differential Scanning Calorimetry. *Chem. Rev.* **2019**, *119* (13), 7848–7939.
- (41) Pooria, G. Differential scanning calorimetry techniques: applications in biology and nanoscience. *J. Biomol. Tech.* **2010**, *21*, 167–193.
- (42) Clas, S. D.; Dalton, C. R.; Hancock, B. C. Differential scanning calorimetry: applications in drug development. *Pharm. Sci. Technol. Today* **1999**, 2 (8), 311–320.
- (43) Ahmadi Khoshooei, M.; Fazlollahi, F.; Maham, Y. A review on the application of differential scanning calorimetry (DSC) to petroleum products. *J. Therm. Anal. Calorim.* **2019**, *138* (5), 3455–3484.
- (44) Masierak, W.; Emmler, T.; Gedat, E.; Schreiber, A.; Findenegg, G. H.; Buntkowsky, G. Microcrystallization of Benzene- d6 in

- Mesoporous Silica Revealed by 2 H Solid-State Nuclear Magnetic Resonance. J. Phys. Chem. B 2004, 108 (49), 18890–18896.
- (45) Jayanthi, S.; Kababya, S.; Schmidt, A.; Vega, S. Deuterium MAS NMR and Local Molecular Dynamic Model to Study Adsorption-Desorption Kinetics of a Dipeptide at the Inner Surfaces of SBA-15. *J. Phys. Chem. C* **2016**, 120 (5), 2797–2806.
- (46) Hassan, J. Analysis of 2H NMR spectra of water molecules on the surface of nano-silica material MCM-41: Deconvolution of the signal into a Lorentzian and a powder pattern line shapes. *Physica B* **2012**, 407 (1), 179–183.
- (47) Krushelnitsky, A.; Reichert, D.; Saalwächter, K. Solid-state NMR approaches to internal dynamics of proteins: from picoseconds to microseconds and seconds. *Acc. Chem. Res.* **2013**, *46* (9), 2028–2036.
- (48) Wang, X.; Lin, K. S. K.; Chan, J. C. C.; Cheng, S. Direct synthesis and catalytic applications of ordered large pore aminopropyl-functionalized SBA-15 mesoporous materials. *J. Phys. Chem. B* **2005**, *109* (5), 1763–1769.
- (49) Zeidan, R. K.; Hwang, S.-J.; Davis, M. E. Multifunctional heterogeneous catalysts: SBA-15-containing primary amines and sulfonic acids. *Angew. Chem., Int. Ed.* **2006**, *45* (38), 6332–6335.
- (50) Brodrecht, M.; Breitzke, H.; Gutmann, T.; Buntkowsky, G. Biofunctionalization of Nano Channels by Direct In-Pore Solid-Phase Peptide Synthesis. *Chem.—Eur. J.* **2018**, *24* (*67*), 17814–17822.
- (51) Weigler, M.; Winter, E.; Kresse, B.; Brodrecht, M.; Buntkowsky, G.; Vogel, M. Static field gradient NMR studies of water diffusion in mesoporous silica. *Phys. Chem. Chem. Phys.* **2020**, 22 (25), 13989–13998.
- (52) Thurber, K. R.; Tycko, R. Measurement of sample temperatures under magic-angle spinning from the chemical shift and spin-lattice relaxation rate of 79Br in KBr powder. *J. Magn. Reson.* **2009**, *196*, 84.
- (53) Vyalikh, A.; Emmler, T.; Shenderovich, I.; Zeng, Y.; Findenegg, G. H.; Buntkowsky, G. 2H-solid state NMR and DSC study of isobutyric acid in mesoporous silica materials. *Phys. Chem. Chem. Phys.* **2007**, 9 (18), 2249–2257.
- (54) de Sousa Amadeu, N.; Grünberg, B.; Frydel, J.; Werner, M.; Limbach, H.-H.; Breitzke, H.; Buntkowsky, G. Melting of Low Molecular Weight Compounds in Confinement Observed by 2 H-Solid State NMR: Biphenyl, a Case Study. *Z. Phys. Chem.* **2012**, 226 (11–12), 1169–1186.
- (55) Massiot, D.; Fayon, F.; Capron, M.; King, I.; Le Calvé, S.; Alonso, B.; Durand, J.-O.; Bujoli, B.; Gan, Z.; Hoatson, G. Modelling one- and two-dimensional solid-state NMR spectra. *Magn. Reson. Chem.* **2002**, *40* (1), 70–76.
- (56) Hoffmann, M. M.; Bothe, S.; Gutmann, T.; Buntkowsky, G. Combining Freezing Point Depression and Self-Diffusion Data for Characterizing Aggregation. *J. Phys. Chem. B* **2018**, *122* (18), 4913–4921.
- (57) Haines, W. M., Ed., Handbook of Chemistry and Physics: A Ready Reference Book of Chemical and Physical Data, 59th, ed.; CRC Press, 1979.
- (58) Findenegg, G. H.; Jähnert, S.; Akcakayiran, D.; Schreiber, A. Freezing and melting of water confined in silica nanopores. *ChemPhysChem* **2008**, 9 (18), 2651–2659.
- (59) Bryant, R. G. The NMR time scale. *J. Chem. Educ.* **1983**, *60* (11), 933.
- (60) Hologne, M.; Hirschinger, J. J. Molecular dynamics as studied by static-powder and magic-angle spinning 2H NMR. *Solid State Nucl. Magn. Reson.* **2004**, *26* (1), 1–10.
- (61) Buntkowsky, G.; Breitzke, H.; Adamczyk, A.; Roelofs, F.; Emmler, T.; Gedat, E.; Grünberg, B.; Xu, Y.; Limbach, H.-H.; Shenderovich, I.; Vyalikh, A.; Findenegg, G. Structural and dynamical properties of guest molecules confined in mesoporous silica materials revealed by NMR. *Phys. Chem. Chem. Phys.* **2007**, *9* (35), 4843–4853.
- (62) Doadrio, A. L.; Sánchez-Montero, J. M.; Doadrio, J. C.; Salinas, A. J.; Vallet-Regí, M. A molecular model to explain the controlled release from SBA-15 functionalized with APTES. *Microporous Mesoporous Mater.* **2014**, 195, 43–49.
- (63) Rössler, E.; Taupitz, M.; Börner, K.; Schulz, M.; Vieth, H.-M. A simple method analyzing 2 H nuclear magnetic resonance line shapes to

- determine the activation energy distribution of mobile guest molecules in disordered systems. *J. Chem. Phys.* **1990**, 92 (10), 5847–5855.
- (64) Vyalikh, A.; Emmler, T.; Gedat, E.; Shenderovich, I.; Findenegg, G. H.; Limbach, H.-H.; Buntkowsky, G. Evidence of microphase separation in controlled pore glasses. *Solid State Nucl. Magn. Reson.* **2005**, 28 (2–4), 117–124.
- (65) Grünberg, B.; Grünberg, A.; Limbach, H.-H.; Buntkowsky, G. Melting of Naphthalene Confined in Mesoporous Silica MCM-41. *Appl. Magn. Reson.* **2013**, *44* (1–2), 189–201.
- (66) Vogel, M. NMR studies on simple liquids in confinement. *Eur. Phys. J. Spec. Top.* **2010**, *189* (1), 47–64.
- (67) Delle Piane, M.; Corno, M.; Ugliengo, P. Propionic acid derivatives confined in mesoporous silica: monomers or dimers? The case of ibuprofen investigated by static and dynamic ab initio simulations. *Theor. Chem. Acc.* **2016**, *135* (3), 53.